DOI: 10.26599/FSHW.2026.9251259

Contents lists available at SciOpen

Food Science and Human Wellness

journal homepage: https://www.sciopen.com/journal/2097-0765

China Food Publishing Co.

A pH-stimulated responsive micro-drug delivery system loaded with gastrodin that improves type 2 diabetes

Yan-Fei Li[1*], Qiong Shen[2*], Jian-Qiang Wang[3], De-Yang Huo[3], Xiao-Xia Cai[1], Kai Zhou[1], Wei Li[3 *]

[1] *College of Pharmaceutical Sciences, Guizhou University of Traditional Chinese Medicine, Guiyang 550025, China*

[2] *College of Food and Health, Zhejiang A & F University, Hangzhou, Zhejiang, 311300, China*

[3] *College of Chinese Medicinal Materials, Jilin Agricultural University, Changchun 130118, China*

ABSTRACT: Type 2 diabetes mellitus (T2DM) is a rapidly increasing global metabolic disease. The development of effective oral hypoglycemic agents, primarily derived from natural compounds, remains a significant challenge. In this study, we developed pH-responsive sodium alginate (SA) microspheres combined with low methoxy pectin (LMP) that are loaded with gastrodin (Gas) (denoted as Gas@MPs) and successfully delivered Gas to the gut for controlled release. Our in vitro research results indicate that Gas can effectively escape from cellular lysosomes into the cytoplasm, be efficiently absorbed by cells, and exhibit remarkable antioxidant properties. Furthermore, in vitro simulations demonstrated that Gas@MPs effectively prevents gastric juice from interfering with intestinal fluid release. Importantly, Gas@MPs significantly improved the regulation of blood glucose levels and restored impaired islet function in STZ-induced diabetic mice. Additionally, Gas@MPs effectively mitigated insulin resistance and promoted glycogen synthesis by modulating the expression of proteins related to GSK3-β, Nrf2, HO-1, Glut2, and IRS-1 in the pancreatic tissue of diabetic mice. Notably, Gas@MPs also effectively reversed the dysregulation of the gut microenvironment. In conclusion, our research suggests that the oral administration of Gas@MPs represents a promising strategy for alleviating T2DM symptoms and offers new insights into the development of innovative oral natural hypoglycemic agents for the treatment of T2DM.

Keywords: Type 2 diabetes mellitus; Gastrodin; pH-responsive; Insulin resistance; Oral natural hypoglycemic agents

1. Introduction

Diabetes has emerged as a global epidemic, presenting a significant challenge to healthcare systems worldwide [1,2]. The international diabetes federation estimates that over 580 million individuals currently have diabetes, with projections indicating this number could rise to 800 million by 2050 [3-5]. Type 2 diabetes mellitus (T2DM) arises from the combined effects of insulin resistance and impaired insulin secretion. Complications associated with diabetes, including cardiovascular diseases, kidney disorders, neuropathy, and retinopathy, severely impact patients' quality of life and contribute to increased morbidity and mortality, thereby imposing a substantial economic burden on global healthcare systems [6,7]. Currently, pharmacological interventions for diabetes management primarily focus on insulin and other chemically synthesized

***Corresponding author**
15764380153@163.com,shenqiong@zafu.edu.cn,liwei7727@126.com

Received 24 December 2025
Received in revised from 10 February 2026
Accepted 10 April 2026

hypoglycemic agents [8]. However, the use of these synthetic drugs is constrained by various limitations. For example, insulin cannot be administered orally due to its instability in the gastrointestinal tract. Additionally, the low bioavailability resulting from poor targeting is a significant limitation for most hypoglycemic medications [9,10]. Consequently, there is an urgent need to explore and develop drug delivery systems that are primarily based on natural compounds and are highly efficient, to enhance the efficacy and safety of existing hypoglycemic drugs.

Gastrodin (Gas) is a natural compound extracted from the dried tubers of the Chinese herbal medicine *Gastrodia elata*, known for its antioxidative, antidiabetic, and antiviral properties [11-14]. However, like many natural compounds, when administered orally, it encounters a complex gastrointestinal environment characterized by degradation from gastric acid and enzymes, which prevents it from reaching the intestine to exert its intended functions [15]. To address this challenge, we developed and optimized a pH-responsive microsphere composed of low-methoxy pectin (LMP) combined with alginate [16-19], aimed at achieving targeted delivery of Gas for intestinal disintegration and release. As a revolutionary drug delivery system (DDS), drug-loaded microspheres are micron-sized spheres (1-1000 μm) constructed from biodegradable polymers, including hyaluronic acid (HA), chitosan, and LMP. These microspheres address the issues of low bioavailability and poor targeting associated with traditional drug delivery methods [20-22]. Their primary advantage lies in the ability to adjust particle size (ranging from nanometers to micrometers) and structural properties (such as the inflammatory targeting capabilities of HA), enabling precise controlled release. Additionally, they protect unstable drugs, including natural compounds, peptides, and nucleic acids, from enzymatic hydrolysis [23-26].

In our research, we first demonstrated that Gas exhibits excellent lysosomal escape performance and is effectively absorbed by cells, thereby displaying significant antioxidant activity. In terms of in vivo studies, we developed and optimized a drug-loaded microsphere with pH-responsive release capabilities, which minimizes the decomposition of Gas in gastric acid, ensures targeted intestinal release, and achieves an effective therapeutic effect of Gas on diabetic disorders. This novel targeted delivery strategy is anticipated to provide more effective and well-tolerated treatment options for diabetic patients and presents promising prospects for the application of Gas.

2. Materials and methods

2.1 Materials

Gastrodin (Gas, purity ≥ 99%) and streptozotocin (STZ, purity ≥ 99.0%) were sourced from Shanghai Macklin Bio-chem Co., Ltd. (Shanghai, China). Low-methoxy pectin (LMP, purity ≥ 99%), alginate (purity ≥ 90%, β-D-mannuronic/α-L-guluronic ratio = 1:2), and palmitic acid (PA, purity ≥ 99.0%) were obtained from Shanghai Aladdin Bio-chem Technology Co., Ltd. (Shanghai, China). Lyso-Tracker Red (C1046) was acquired from Beyotime Biotechnology Co., Ltd. (Shanghai, China). The total cholesterol (TC) assay kit (A-111-1), triglyceride (TG) assay kit (A-110-1), high-density lipoprotein cholesterol (HDL-C) assay kit (A112-

1-1), and low-density lipoprotein cholesterol (LDL-C) assay kit (A113-1-1) were purchased from Nanjing Jiancheng Bioengineering Institute (Nanjing, China). The interleukin-1β (IL-1β) assay kit (ml063132) and tumor necrosis factor (TNF-α) assay kit (H052) were obtained from Shanghai Enzyme-linked Biotechnology Co., Ltd. (Shanghai, China). Hematoxylin and Eosin (H&E), terminal deoxynucleotidyl transferase (TdT)-mediated dUTP nick end labeling (TUNEL), Masson's trichrome staining, immunohistochemistry (IHC), and immunofluorescence (IFC) were acquired from Servicebio Co., Ltd. (Wuhan, China). The bicinchoninic acid (BCA) assay kit (PC0020) and Hoechst 33342 assay kit (G023-1-1) were obtained from Beijing Soleibao Technology Co., Ltd. (Beijing, China). The primary antibodies used were as follows: HO-1 (1:100, Abcam, UK), Nrf2 (1:500, Abcam, UK), GAPDH (1:500, Beyotime, China), MAPK (1:500, Beyotime, China), IRS1 (1:1000, Beyotime, China), Glut2 (1:500, Abcam, UK), and GSK3-β (1:500, Abcam, UK).

2.2 Preparation of Microgels

Based on previous literature and multiple experiments, microspheres were prepared using different concentrations of SA and LMP. The results showed that at a concentration of 1.5% for SA and 0.5% for LMP, the microspheres exhibited a complete and uniform spherical shape. After determining the optimal concentration, further experiments indicated that to prepare the best microspheres, the following conditions were required: an injection distance of 16 cm, a voltage of 16 kV, and the optimal $CaCl_2$ concentration of 2%.

2.3 Drug loading and encapsulation rate

Under the aforementioned optimal conditions, we can add the specified Gas to obtain the Gas@MPs microspheres with the required concentration for our experiment. During our production process, all the added Gas can be effectively loaded into the microspheres, so the encapsulation rate is theoretically 100%. Regarding the drug loading capacity, we analyzed it using the HPLC method. We precisely weighed 1 gram of Gas@MPs, thoroughly ground it, and then added 10 mL of ethanol for dissolution. We took 200 μL for the HPLC test. The conditions were: C18 chromatographic column, mobile phase of (acetonitrile: water = 3:97), flow rate of 1.0 mL/min, column temperature of 37 ℃, injection volume of 10 μL, and detection wavelength of 220 nm. Finally, the drug loading capacity was calculated to be approximately 35.6%.

2.4 Culturing L-02 cells and Establishing a Hyperglycemic Model

Following the cell resuscitation, the cells were cultured in a hyperglycemic medium. Once successful passage was achieved, palmitic acid (PA, 200 μmol/mL) was utilized to create a hyperglycemic damage model [27].

2.5 Antioxidant Activity Test of Gas@MPs

The free radical scavenging activity was assessed using the DPPH method. Various concentrations of Gas solution (10, 20, 40, 60, 80, 100, and 120 μg/mL) were combined with 200 μL of DPPH at a concentration of 0.1 mmol/L and incubated at 37 ℃ in a 96-well plate for 30 minutes. Subsequently, the absorbance of each

sample was measured at 517 nm [28]. The formula for calculating the DPPH free radical scavenging activity is as follows:

$$\text{Free radical scavenging activity (\%)}=\frac{\text{A1-A2}}{\text{A1}}\times 100\%$$

where A1 is the absorbance value of the control and A2 is the absorbance value of the sample group.

2.6 Lysosome Escape and Cell Uptake Assessment

In brief, 50 microliters of a FITC dimethyl sulfoxide solution were added to 5 mL of the Gas solution, which was then stirred in the dark for 12 hours. Subsequently, the FITC-Gas was placed in a 500-mesh dialysis bag and subjected to freeze-drying for subsequent cell uptake experiments. The FITC-Gas was treated with cultured L-02 cells for 2, 4, and 8 hours, respectively. After incubation, the cells were washed three times with PBS, treated with LysoTracker Red for 45 minutes, fixed with 4% paraformaldehyde for 15 minutes, and then washed with PBS again. Cell nuclei were stained with DAPI, and cell imaging was captured using a laser confocal microscope [29]. Additionally, L-02 cells were cultured in a dish for 24 hours, followed by treatment with the FITC-Gas for 2, 4, and 6 hours, respectively, and then washed three times with PBS. The cells were subsequently fixed with 4% paraformaldehyde for 45 minutes and washed three times with PBS. Afterward, they were stained with DAPI for 30 minutes and washed three times with PBS. Finally, the uptake ability at different time points was observed using a laser confocal microscope.

2.7 Antioxidant and Anti-Apoptosis Research

The inhibitory effect of reactive oxygen species (ROS) on L-02 cells was investigated. In a 12-well plate, with a cell density of 1×10^5 cells/mL, the cells were treated with 200 μmol/L of palmitic acid (PA) for 24 hours. Subsequently, 60 and 120 μg/mL of Gas were added to the cells, and the culture was continued for an additional 24 hours. Following this, 1 mL of serum-free medium (without serum) containing DCFH-DA (10 μg/mL) was added to a 6-well plate and incubated according to the manufacturer's instructions. The cells were then washed three times with serum-free medium. Fluorescence imaging and co-localization analysis were performed using a laser scanning confocal microscope and ImageJ software. Additionally, the cells were cultured following the aforementioned procedure. After incubation, the cells were treated with PA for 24 hours, after which 60 and 120 μg/mL of Gas were added. The excess medium was then removed, and the cells were stained using an apoptosis/necrosis kit. Specifically, 5 μL of Hoechst 33342 and 5 μL of propidium iodide (PI) were added to each well containing 1 mL of cell staining buffer and incubated at 4 ℃ for 45 minutes [30]. The cells were then washed three times with PBS, and the fluorescence imaging and analysis methods were consistent with those described previously.

2.8 Microstructure Observation of Gas@MPs

The morphology of the Gas@MPs was examined using transmission electron microscopy (TEM, JEM-2100, Hitachi, Tokyo, Japan). The sample solution was evenly distributed onto a copper grid, stained with 2%

phosphotungstic acid, and air-dried at room temperature. TEM observation was carried out at 100 kV. In addition, scanning electron microscopy (SEM, JSM-7800F, Hitachi, Tokyo, Japan) was used to investigate the microstructure of the Gas@MPs.

2.9 HPLC analysis of Gas

C18 (4.6 mm × 150 mm, 5 μm) chromatographic column, mobile phase consisting of 0.1% phosphoric acid solution-acetonitrile (97:3), detection wavelength of 220 nm, column temperature of 25 ℃, flow rate of 1.0 mL/min.

2.10 Stability assessment of Gas@MPs

Firstly, Gas@MPs microspheres were placed in water for 72 hours, and the particle size of the microspheres was evaluated at 0, 6, 12, 24, 48, and 72 hour time points. Additionally, we further investigated the stability of Gas@MPs in gastrointestinal fluid, and the particle size of the microspheres was evaluated at 0, 2, 4, 6, 8, and 10 hour time points.

2.11 In Vivo Anti-Diabetic Experiments

Eight-week-old Balb/c male mice (weight (26 ± 3) g) were purchased from Changsheng Biological Co., Ltd., accompanied by a Certificate of Quality No. SYXK (Gui) 2025-0011 (GuiYang, China). All experimental procedures involving animals were conducted in strict accordance with the Guide for the Care and Use of Laboratory Animals and complied with the Regulations of Experimental Animal Administration issued by the Ethical Committee for Laboratory Animals at Guizhou University of Chinese Medicine (Permit No.: 202426361104364868). All groups, except for the normal group, were subjected to a high-fat diet for 7 days. To induce a diabetic model, mice received three successive intraperitoneal injections of STZ (35 mg/kg), administered at two-day intervals. Mice exhibiting fasting blood glucose levels consistently at or above 11.1 mmol/L for 7 consecutive days were classified as diabetic and qualified for subsequent experimentation. In this study, we investigated the effects of various treatments on diabetic mice. The subjects were randomly assigned to five distinct groups, each consisting of ten mice. The designated groups included: the blank group (normal saline), the STZ group (STZ injection), the free Gas group (150 mg/kg), the Gas@MPs group (Contains 150 mg/kg of Gas), and the metformin group (150 mg/kg). Throughout the study, the mice received daily intragastric administration, with continuous blood glucose monitoring. Following a 60-day intervention period, the mice were humanely euthanized, and their blood samples were collected for further analysis.

2.12 Tissue Section Staining, Immunohistochemistry and Immunofluorescence Analysis

The liver, kidney, and pancreas tissues were initially fixed in a 4% paraformaldehyde solution. Subsequently, the tissues were embedded in paraffin and sectioned into full-thickness slices of 5 μm. These sections underwent a series of deparaffinization steps, including a 15-minute wash in xylene, followed by 15-minute washes in 95%, 75%, and 50% ethanol. Finally, the sections were stained with hematoxylin-eosin

(H&E) and Masson trichrome according to established protocols. Immunohistochemical (IHC) staining was performed following the manufacturer's protocols (Boster, China). Pancreatic sections were incubated overnight at 4 ℃ with anti-insulin mouse monoclonal antibody (mAb) (Servicebio, GB11097) and anti-glucagon mouse mAb (Servicebio, GB12097). After washing, the sections were incubated with horseradish peroxidase (HRP)-conjugated goat anti-mouse IgG (Servicebio, GB23301). The slides were then covered, and images were captured using a fluorescence microscope (Nikon, Eclipse C1, Japan). In this study, immunohistofluorescence (IFC) was conducted on pancreatic sections. Initially, the sections were incubated at 37 ℃ for 0.5 hours with anti-insulin mouse mAb (Servicebio, GB11097). They were subsequently incubated overnight at 4 ℃ with anti-glucagon mouse mAb (Servicebio, GB12097). Following this, FITC-conjugated goat anti-mouse IgG (Servicebio, GB22301) was added to the pancreatic tissue and incubated in the dark for 1.5 hours. Finally, the tissue was counterstained with 4′,6-diamidino-2-phenylindole (DAPI, Servicebio, GDP1024) for nuclear visualization. The slides were then covered, and images were captured using a fluorescence microscope (Nikon, Eclipse C1, Japan).

2.13 Assessment of Biochemical Parameters

Firstly, we measured the lipid indicators such as total cholesterol (TC), triglycerides (TG), low-density lipoprotein cholesterol (LDL-C), and high-density lipoprotein cholesterol (HDL-C) in pancreatic tissue. We also determined the concentrations of inflammatory factors, IL-1β and TNF-α, in the pancreatic tissue using an enzyme-linked immunosorbent assay kit. All operations were conducted carefully following the guidelines provided in the kit instructions.

2.14 Optimization of Preparation Technology of Microspheres

The influence of the concentration ratio of SA to LMP on the morphology of microspheres. Firstly, the effects of injection distance (4, 8, 12, 16 and 20 cm), applied voltage (4, 8, 12, 16 and 20 kV), and $CaCl_2$ concentration (0.5, 1, 1.5, 2 and 2.5%) on the microsphere preparation process were investigated.

2.15 Biological safety assessment

The mice were divided into four groups: the blank group, the free Gas group, the Gas@MPs group, and the metformin group. After being fed for 30 days, the mice were dissected and blood serum samples and tissue samples were collected. Firstly, H&E staining was performed on the main metabolic organs (heart, liver, spleen, lung, and kidney) to assess their condition. Then, blood routine analysis was conducted on the blood serum samples in accordance with the instructions of the kit. The results of these two evaluations were used to jointly assess the biological safety of Gas@MPs.

2.16 Analysis of the Intestinal Microenvironment

Before dissecting the mice, we conducted 16S rRNA sequencing on their fecal samples to deeply investigate the changes in the intestinal microbial communities of different groups of mice. This method

involved extracting genomic DNA, performing PCR amplification, fluorescence quantification, constructing Miseq libraries, and subsequent Miseq sequencing. The subsequent analysis focused on the species heterogeneity, structural composition, and differences of the intestinal microbial communities in mice.

2.17 Western Blotting Analysis

In this investigation, proteins were extracted from pancreatic tissues or cells using the radioimmunoprecipitation assay (RIPA) lysis buffer and subsequently quantified via the bicinchoninic acid (BCA) method. To ensure uniformity across the samples, equal quantities of protein (50 μg/lane) were loaded onto 12% SDS-PAGE gels and transferred to polyvinylidene difluoride (PVDF) membranes. Initially, the membranes were blocked with 3% bovine serum albumin (BSA) in tris-buffered saline (TBS) containing 0.05% Tween-20 and incubated at room temperature for 1.5 hours. Following this, primary antibodies were applied, and the membranes were incubated overnight at 4 ℃. Subsequently, the membranes were washed three times with tris-buffered saline-Tween (TBST) for 8 minutes each. Ultimately, the membranes were exposed to secondary antibodies at room temperature for one hour [31]. In the final analysis, protein bands were detected using enhanced chemiluminescence (ECL) from Pierce Chemical Co. in Rockford, IL, USA, and visualized using the ChemiDoc Touch detection system supplied by Bio-Rad in the USA. Finally, the band intensity was evaluated using Image Plus 6.0 software.

2.18 Statistical analysis

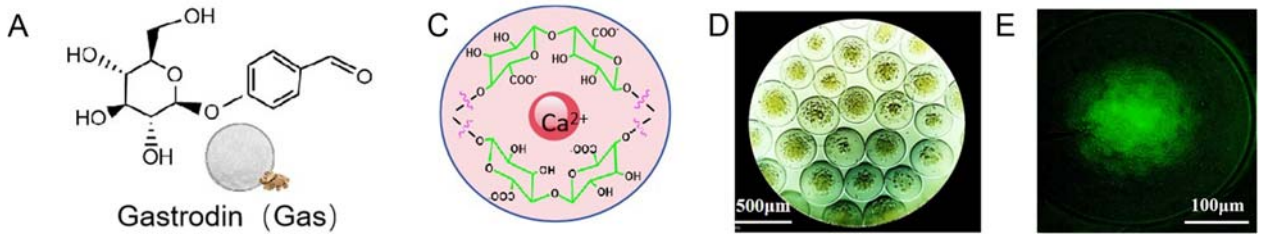
All experimental data were represented as mean ± standard deviation (SD). Significance analysis between groups was performed using one-way analysis of variance (ANOVA). The level of significance was represented as follows: ns indicates $P > 0.05$ (no significance), $^{*}P < 0.05$ indicates significance, $^{**}P < 0.01$ indicates high significance, and $^{***}P < 0.001$ indicates very high significance. Data graphing analysis was conducted using GraphPad Prism 8.0 and Origin 2019.

3. Results and Discussion

3.1 Gas@MPs Characterization and pH Responsiveness Analysis

SA microspheres are biopolymer materials derived from natural seaweed, characterized by excellent biocompatibility and the absence of rejection reactions. Sodium alginate microspheres serve as drug carriers, capable of encapsulating drugs within their structure, thereby facilitating slow drug release and achieving targeted therapeutic effects. These microspheres protect drugs from degradation by digestive enzymes and the immune system, thereby enhancing drug stability. Through surface modification, sodium alginate microspheres can achieve targeted delivery to specific tissues and organs, accurately directing drugs to lesion sites and improving therapeutic efficacy. The chemical formula of Gas is illustrated in Figure 1A. We synthesized drug-loaded microspheres (Gas@MPs) by electrostatic spraying a $CaCl_2$ solution, incorporating gas into a solution of sodium alginate (SA) and low-methoxy pectin (LMP) in a specific ratio, as depicted in Figure 1B. The formation mechanism involves calcium ions forming ionic bonds with the carboxylic acid

groups in sodium alginate molecules, resulting in a stable three-dimensional network structure (Figure 1C). After substituting FITC with Gas to create microspheres, we employed both a standard microscope and an inverted fluorescence microscope to simulate the internal environment of the microspheres. It was clearly observed that the microspheres effectively encapsulated the drug (Figure 1D,E), demonstrating the feasibility of preparing Gas@MPs. To further evaluate the scientific characteristics of the gas encapsulated in the microspheres, we employed scanning electron microscopy (SEM) and energy dispersive spectroscopy (EDS) to analyze both the overall and cross-sectional morphology of the prepared Gas@MPs microspheres (Figure 1F-H). Our analysis revealed that the microspheres contained calcium (Ca), chloride (Cl), carbon (C), and oxygen (O) elements, consistent with the fundamental components of the raw materials utilized. Notably, the cross-sectional examination disclosed a porous internal structure, which is conducive to effective drug storage (Figure 1I,J). Furthermore, we selected 100 Gas@MPs for particle size analysis, determining that the microspheres exhibited an average particle size of (356 ± 12.1) μm. Previous studies have indicated that SA microgels exhibit pH responsiveness, attributable to the inherent structure of SA. In acidic environments, the interior of the microgels becomes compact, hindering drug release. Conversely, under weakly alkaline or alkaline conditions, they swell and may disintegrate, thereby facilitating drug release. Accordingly, we first assessed the stability of the prepared Gas@MPs microspheres in water, observing no significant change in particle size over a 72-hour period (Figure 1L). Additionally, we investigated their absorption and digestion in the gastrointestinal tract using artificial simulated gastroenteric fluid (SGF), finding that Gas@MPs demonstrated relative stability in artificial simulated gastric fluid (Figure 1M). In artificial simulated colonic fluid (SCF), swelling occurred over a defined period, ultimately leading to disintegration (Figure 1N). In order to determine whether Gas or its aglycone form was present in the intestinal tract of mice after oral gavage of Gas@MPs, we used HPLC to analyze the components in the intestinal tract of the mice 6 hours after oral administration of Gas@MPs (Figure S1). The results showed that the aglycone form of Gas (orthohydroxybenzyl alcohol) was not detected.



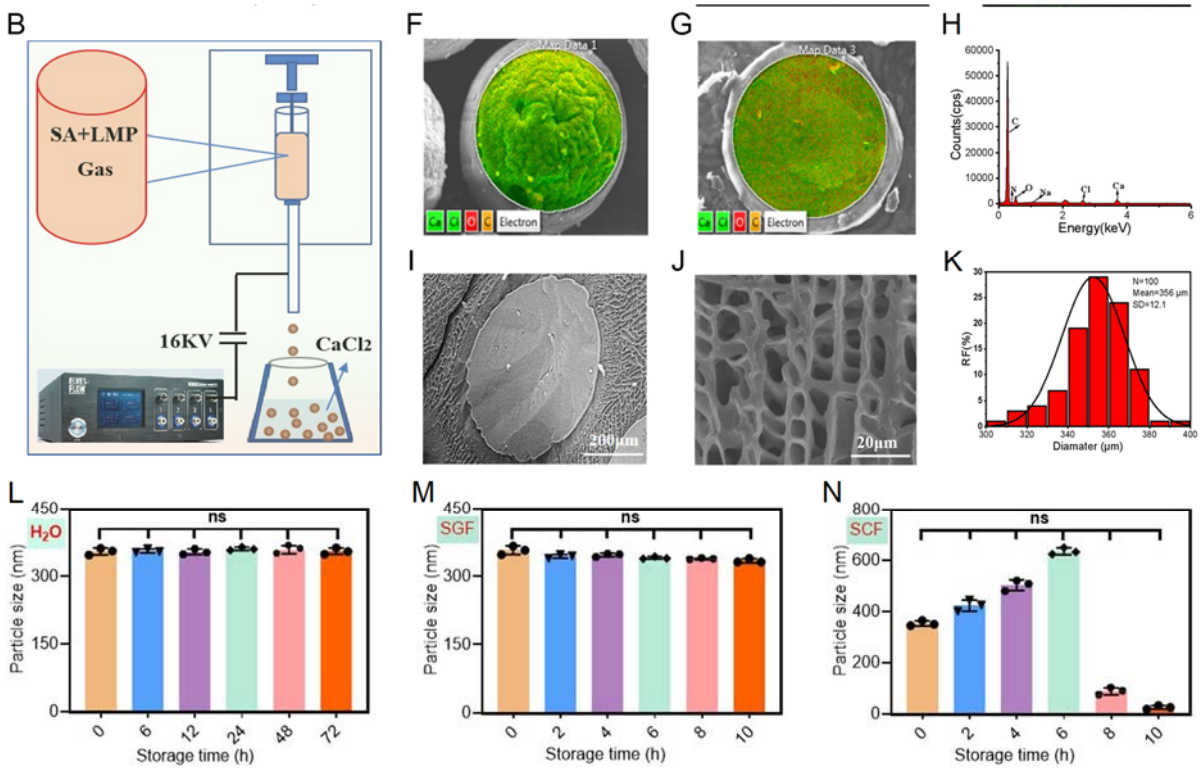
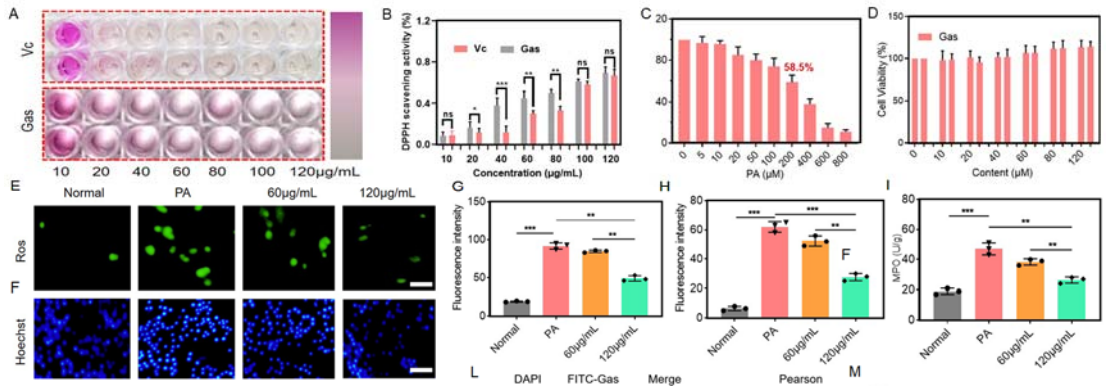


Fig.1 Characterization and pH Responsiveness Analysis of Gas@MPs. (A) Chemical structural formula of Gas. (B) Flowchart illustrating the preparation of Gas@MPs. (C) Principles underlying the preparation of Gas@MPs. (D) Microscope image depicting Gas@MPs, with a scale of 500 μm. (E) Inverted fluorescence microscope image of Gas@MPs, with a scale of 100 μm. (F-H) Scanning Electron Microscopy (SEM) and Energy Dispersive Spectroscopy (EDS) images of Gas@MPs. (I,J) SEM cross-sectional analysis of Gas@MPs, with a scale of 200 μm and 20 μm. (K) Particle size distribution of Gas@MPs. (L-N) Stability and pH responsiveness of Gas@MPs in H_2O, simulated gastric fluid (SGF), and simulated colonic fluid (SCF).

3.2 Evaluation of the Antioxidant Stress Performance of Gas

In this study, DPPH was employed to assess the in vitro antioxidant activity of Gas, with the color change serving as an additional indicator of its antioxidant capacity [32]. The results indicate that the antioxidant activity of Gas increases in a concentration-dependent manner. As the concentration of Gas rises, the solution's color transitions from pink to yellow (Figure 2A). Notably, at a concentration of 120 μg/mL, the clearance rate of DPPH radicals by Gas reached 68.6% (Figure 2B). The favorable biological safety profile of Gas supports its potential applications. A concentration gradient analysis revealed that Gas exhibits no toxic or side effects on normal human liver cells. Conversely, treatment with Gas appears to promote cell proliferation (Figure 2D). Based on our findings, we hypothesize that Gas possesses a potential reversing effect on cell damage. The liver is critical in glucose metabolism. Palmitic acid (PA), a prevalent fatty acid found in high-fat diets and obesity [33-35]. is known to induce insulin resistance and cellular damage. In this study, we aim to investigate whether Gas can reverse PA-induced mitochondrial dysfunction and enhance glucose uptake in hepatocytes. We established a hyperglycemic cell injury model using human normal liver cells (L-02 cells) induced by PA [36]. Consequently, PA was utilized to induce injury in L-02 cells. Our results indicated that at a PA dose of 200 μmol/L, cell viability decreased to 58.5%, highlighting the significant damaging effect of PA on these cells (Figure 2C). Furthermore, we assessed Gas's ability to mitigate PA-induced cellular oxidation and apoptosis. To evaluate this potential, we employed reactive oxygen species (ROS) and Hoechst

33342 staining, a nucleic acid dye commonly used for staining chromosomes and cell nuclei. Following PA induction, apoptotic cells exhibited dense bright blue staining. However, after treatment with Gas, the number of apoptotic cells decreased significantly. The apoptotic cell count in the Gas@MPs treatment group was comparable to that of the control group, further demonstrating that Gas effectively reduced cellular oxidation and apoptosis (Figure 2E-F). The detection results of MPO, MDA, and GSH further confirmed that Gas effectively improves PA-induced cellular oxidation (Figure 2I-K). The aforementioned research has verified the protective effect of Gas on L-02 cells; however, effective drug uptake is essential for it to exert its corresponding physiological functions. To investigate this, Gas was labeled with the fluorescent probe FITC (green fluorescence), and its uptake in L-02 cells was observed under a fluorescence microscope. After a 2-hour incubation, a significant amount of green fluorescence was detected, with a Pearson coefficient of 41.64. The fluorescence intensity significantly increased after 6 hours, reaching a Pearson coefficient of 63.39 (Figure 2L,M), indicating that Gas can be effectively absorbed and taken up by L-02 cells. Previous studies have emphasized the importance of the timely escape of lysosomes from endocytic nanomedicines to prevent premature degradation. To elucidate the intracellular behavior of Gas, the LysoTracker Red probe was utilized to assess its ability to escape from lysosomes. As shown in Figure 2N, the initial overlap between the red (lysosomal) and green (nanoparticle) fluorescence is evident. This co-localization manifests as orange fluorescence, which intensifies between 2 and 4 hours, with the Pearson correlation coefficient increasing from 26.09 to 80.05. However, the transformation observed at the 8-hour mark shows a reduction in orange fluorescence, accompanied by a shift towards distinct red and green fluorescence, indicating that Gas begins to escape from the lysosome. The Pearson coefficient decreased to 67.76, confirming this escape (Figure 2N,O). The schematic diagram illustrating this escape is shown in Figure 2P. Although our research initially indicates that Gas possesses certain antioxidant properties, its specific mechanism of action remains to be elucidated. In this study, we employed immunoimprinting analysis to further assess the expression levels of related proteins Nrf2, Nox4, and HO-1. Our findings demonstrate that Gas treatment effectively mitigates the abnormal expression of Nox4 protein induced by PA (Figure 2Q-T) while simultaneously enhancing the expression levels of Nrf2 and HO-1 proteins. In conclusion, the protective effect of Gas on L-02 cells may be mediated through the regulation of the Nrf2/Nox4/HO-1 signaling pathway.



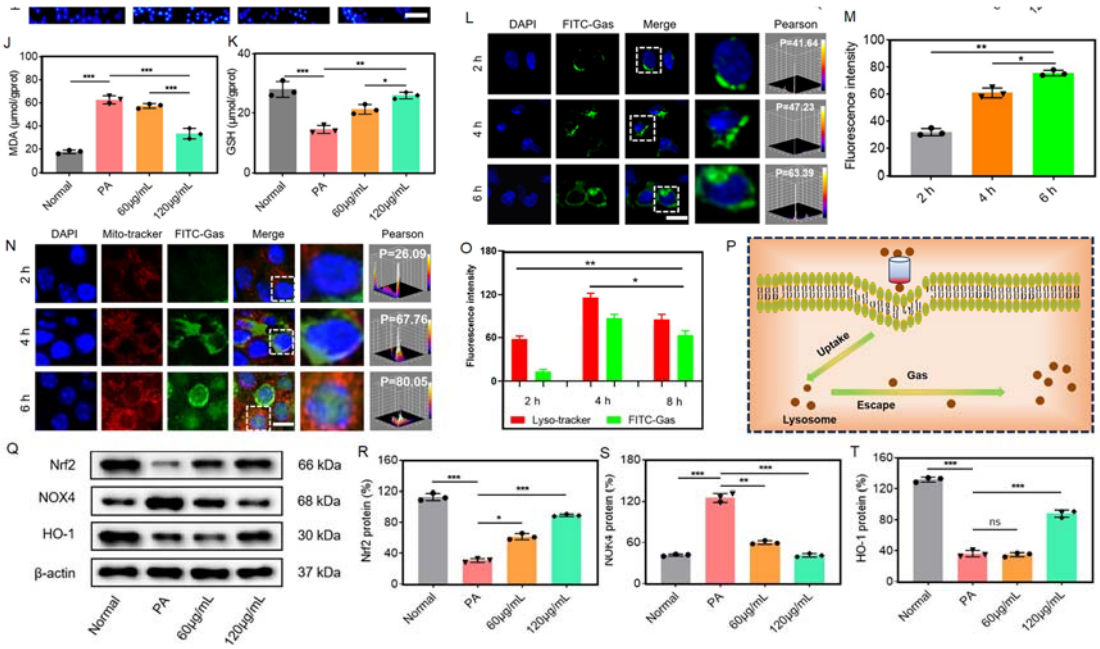
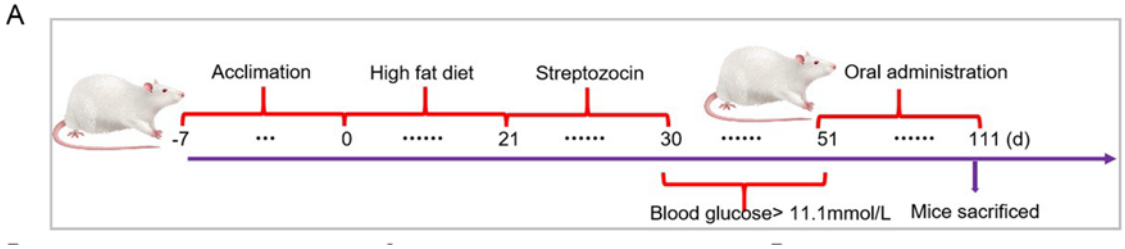


Fig.2 Gas has been shown to mitigate PA-induced mitochondrial dysfunction and oxidative stress in cells. (A) DPPH assay results, the test concentration range is 10 - 120 μg/mL. (B) Quantitative analysis of DPPH levels. (C) The impact of PA on the viability of L-02 cells. (D) Assessment of the cytotoxicity of Gas. (E) Reactive oxygen species (ROS) analysis. (F) Hoechst 33342 staining analysis. (G, H) Quantitative assessment of ROS and Hoechst 33342 staining. (I, K) Evaluation of antioxidant activity through measurements of myeloperoxidase (MPO), malondialdehyde (MDA), and glutathione (GSH) levels. (L, M) Analysis of cellular uptake at various time intervals (2, 4, and 6 hours), with a scale of 10 μm. (N-P) Assessment of lysosomal escape, with a scale of 10 μm. (Q) Expression levels of Nrf2, Nox4, and HO-1 proteins. Quantitative analysis of the expression levels of (R-T) Nrf2, Nox4, and HO-1 proteins. The data were presented as mean ± SD (n = 3-6), ns means $P > 0.05$ (no significance), * $P < 0.05$, ** $P < 0.01$, *** $P < 0.001$.

3.3 Gas@MPs Effectively Achieve Intestinal Release and Improve Abnormal Blood Sugar in Mice

The pH responsiveness of Gas@MPs in gastrointestinal fluids was examined using microscopy (Figure 3E, F). The results indicated that Gas@MPs did not exhibit significant changes in gastric fluid within the first six hours; however, a notable expansion was observed in intestinal fluid after 0.5 hours, with the microspheres significantly disintegrating and releasing Gas after three hours. Additionally, the release of Gas from Gas@MPs in gastrointestinal fluids was assessed using high-performance liquid chromatography (HPLC) (Figure 3C), revealing that only trace amounts of Gas (approximately 12.5%) were detected in artificial simulated gastric fluid (SGF) over a period of 20 hours. In contrast, significant release was observed in artificial simulated small intestinal fluid (SIF) and artificial simulated colon fluid (SCF) after 20 hours, with Gas accumulation reaching 84.3%. Furthermore, in vivo pharmacokinetics were employed to compare the absorption and metabolism of Gas and Gas@MPs in mice. The data (Figure 3D) demonstrated that the absorption efficiency of free Gas was very low, with a maximum concentration of only 7.0 μg/mL, whereas Gas@MPs exhibited superior absorption, achieving 13.6 μg/mL. we first calculated the area under the curve (AUC) of the blood drug concentration-time profile after oral administration of free Gas and Gas@MPs, which were 49.3 μg·h/mL and 130.3 μg·h/mL, respectively. This clearly indicates that the effective absorption of Gas was significantly higher when administered as Gas@MPs compared to free Gas. Additionally, we calculated the half-life (t1/2). As shown in the figure, the blood drug concentration was highest at 6 hours, reaching 13.6 μg/mL after oral administration of Gas@MPs, and was 3.1 μg/mL at 18 hours. Therefore, the

elimination rate constant ($K_{Gas@MPs}$) of the drug was (Inco - Inc) / t = (In13.6 - In3.1) / (18 - 6) = 0.123, and the half-life (t1/2) was 0.693 / K = 5.634 hours. Similarly, the K_{Gas} of free Gas was (Inco - Inc) / t = (In4.5 - In1) / (12 - 6) = 0.25, and the t1/2 was 0.693 / K = 2.77 hours. It can be seen that Gas@MPs significantly prolonged the half-life of Gas, indicating that free Gas was eliminated more rapidly in the body, which is due to the fact that the effective amount absorbed through the gastrointestinal tract was low. The calculation of drug clearance (Clearance, CL) is of great significance for pharmacokinetic studies and rational clinical drug use. Based on the dose and AUC, the calculation formula is: CL = Dose / AUC, where CL represents the drug clearance, Dose represents the administered dose, and AUC represents the area under the drug concentration-time curve, that is, the drug exposure. We calculated that $CL_{Gas@MPs}$ = 150 / 130.7 = 1.15, and similarly, CL_{Gas} = 150 / 49.3 = 3.04. Thus, it can be seen that the clearance of free Gas was much higher than that of Gas@MPs, which fully demonstrates the sustained-release performance of Gas@MPs. These findings suggest that Gas@MPs effectively evade degradation in gastric fluid, thereby displaying remarkable pH responsiveness. Diabetes can lead to various complications, not only causing pancreatitis but also diabetes-related liver diseases and kidney diseases [37-40]. Based on this, our aim is to determine the pathological changes in key organs such as the liver, kidneys, and pancreas, and to explore whether Gas@MPs treatment can improve the related pathological conditions. Therefore, we will use hematoxylin-eosin (H&E) staining (Figure 3F) and Masson staining (Figure 3G) on liver, kidney, and pancreas sections respectively. It can be clearly observed that the Gas@MPs treatment group shows a morphology similar to the normal group, with obvious inflammation or fibrosis, indicating that Gas@MPs can reduce the proliferation of collagen fibers, inhibit the inflammatory infiltration of the liver and kidneys, and protect the pancreatic morphology from pancreatic damage caused by STZ (indicated by the black arrows). These results provide strong evidence for the potential of Gas@MPs in alleviating related complications during diabetes treatment. The previous basic research has preliminarily shown that Gas@MPs can effectively protect the main organs affected by diabetes, but the related molecular mechanism still needs to be explored. Our research has revealed that STZ treatment can cause abnormal expression levels of MAPK and NF-κB molecules. After Gas@MPs treatment, this disorder was effectively regulated (Figure 3 H-J). Therefore, we hypothesize that the improvement of diabetes by Gas@MPs may be related to the regulation of the MAPK/NF-κB signaling pathway.



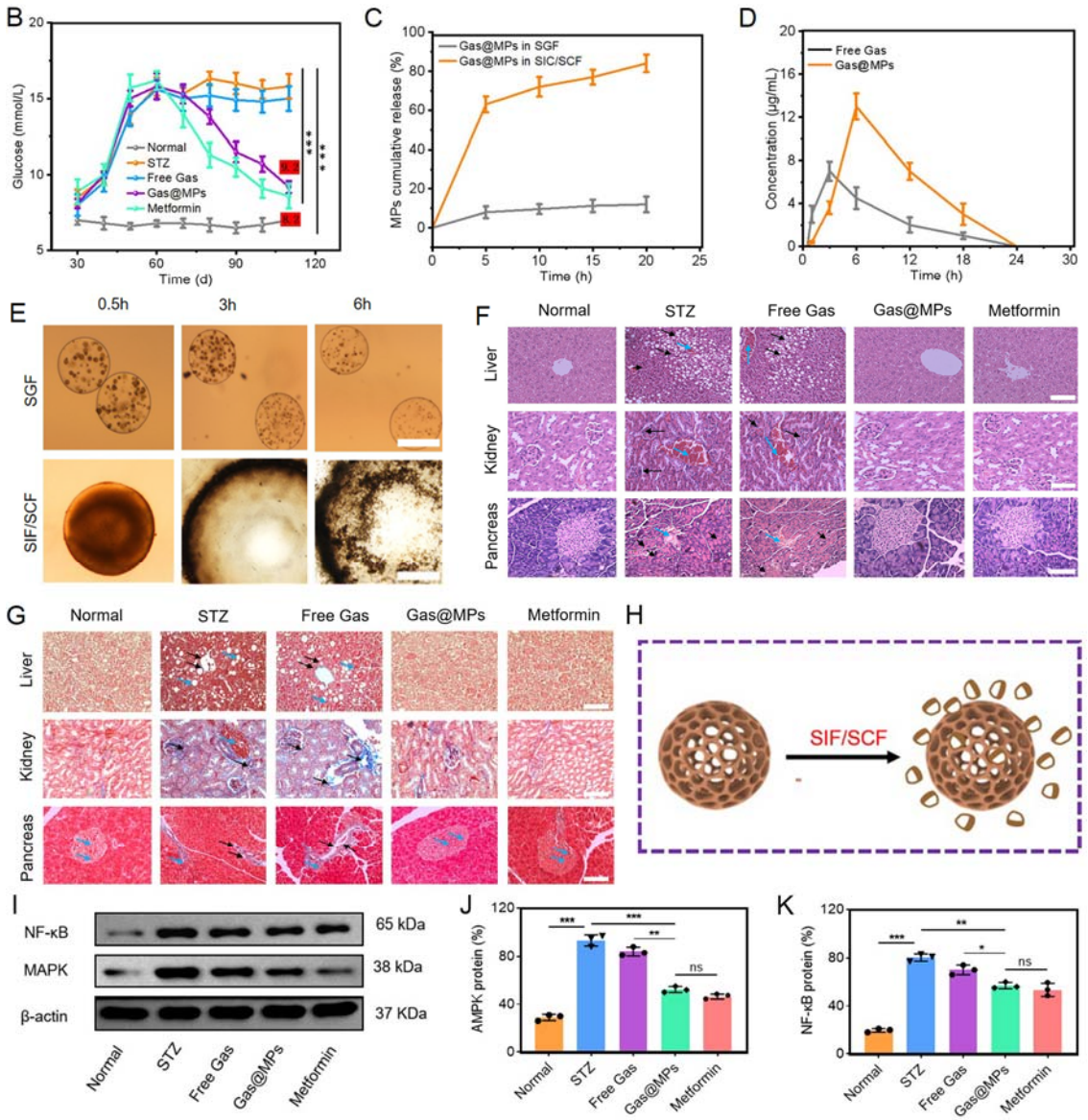
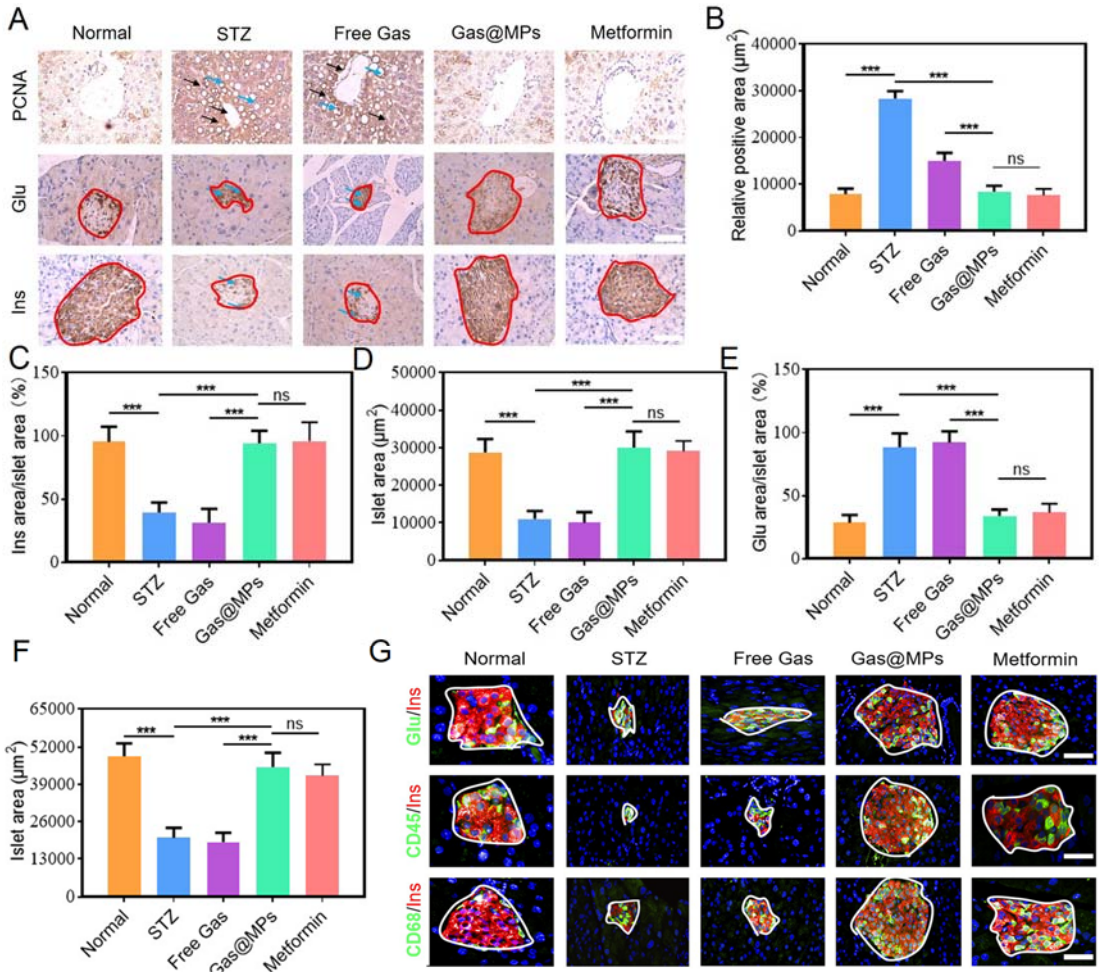


Fig.3 Gas@MPs demonstrate positive effects on diabetic mice. (A) Schematic representation of the feeding and experimental process for T2DM mice. (B) Blood glucose levels in mice were monitored with various drugs at different time intervals. (C) In vitro simulation of Gas release from Gas@MPs. (D) Pharmacokinetic analysis of free Gas and Gas@MPs in vivo. (E) Simulation of the in vitro digestion process using artificial gastrointestinal fluid. Scale bars :300 μm. (F) H&E staining assessment of liver, kidney, and pancreatic tissues, with scale bars set at 200 μm. (G) Masson staining assessment of liver, kidney, and pancreatic tissues, with scale bars set at 200 μm. (H) Diagram illustrating the digestion of Gas@MPs. (I) Western blot analysis to detect the expression levels of NF-κB and MAPK proteins in pancreatic tissue. (J, K) Quantitative analysis of the expression levels of NF-κB and MAPK proteins. The data were presented as mean ± SD (n = 3-8), ns means $P > 0.05$ (no significance), * $P < 0.05$, ** $P < 0.01$, *** $P < 0.001$.

3.4 Gas@MPs Mitigates Diabetes-Related Histological Injury

The tissue sections of the main organs were utilized to demonstrate the protective effects of Gas@MPs on these organs.Type 2 diabetes is a disease characterized by insufficient insulin (Ins) levels and elevated glucagon (Glu) levels [41]. The proliferating cell nuclear antigen (PCNA) is synthesized in the cell nucleus and coexists within it. It is an auxiliary protein of DNA polymerase. Research results indicate that PCNA can serve as an important indicator for assessing abnormal cell proliferation status. During the development of diabetes, as the expression of PCNA gradually increases, the positive cell expression also gradually rises [42,43]. Glu plays a significant role in maintaining normal glucose homeostasis and metabolism, especially in diabetes [44].

Immunohistochemical staining of liver tissue sections revealed that Gas@MPs treatment significantly reduced the expression level of PCNA in the liver, which was lower compared to the other experimental groups. Additionally, Gas@MPs effectively decreased the expression level of Glu and increased the level of Ins in pancreatic tissue. Notably, Gas@MPs significantly restored the morphology and area of islets in the pancreas, effectively improving abnormal blood sugar levels (Figures 4A-E). To further and more intuitively assess the potential positive regulatory effects of Gas@MPs on pancreatic function and morphology, we performed dual staining with Ins (in red) and Glu (in green) on pancreatic sections (Figure 4G). Furthermore, we investigated the invasion of immune cells into the pancreas. Dual staining was performed on pancreatic tissue, using red to depict insulin and green to illustrate the lymphocyte markers CD45 and CD68 [45,46]. As anticipated, no significant green fluorescence from CD45 and CD68 was detected in the pancreas of treated mice, indicating that the degree of immune cell invasion in the mice treated with Gas@MPs was the lowest. In contrast, other groups, particularly those treated with STZ alone and the free Gas treatment group, exhibited severe immune cell invasion, with a more intense green signal. Our observations indicate that the area of the islets in the pancreas treated with Gas@MPs is larger and their shape is more regular. Compared to the control group, the proportion of green fluorescence (representing glucagon) within the entire islet is significantly reduced (Figure 4H).



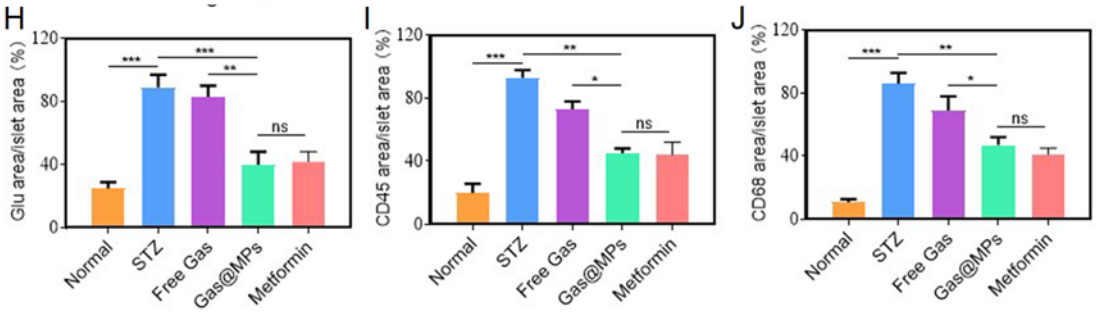


Fig.4 Gas@MPs preserves the morphology and functionality of pancreatic and liver tissues. (A) Immunohistochemical staining was employed to assess the expression levels of PCNA, Insulin (Ins), and Glucose (Glu) in major organs, with scale bars set at 200 μm. (B) A quantitative analysis was conducted on the positive expression of PCNA. (C) The ratio of the area of Insulin to the area of islets within pancreatic tissue was calculated. (D) Immunohistochemical analysis was performed to evaluate the area of islets in relation to Glucose. (E) The ratio of Glucose to the area of islets in pancreatic tissue was determined. (F) Immunohistochemical detection was utilized to assess the area of islets in relation to Insulin. (G) Immunofluorescence staining was conducted to visualize the expression of Insulin, Glucose, CD45 (green), and CD68 (green) in pancreatic tissue, with scale bars set at 200 μm. (H) A quantitative analysis was performed to determine the area ratio of Glucose to islets based on immunofluorescence detection. (I, J) Quantitative analyses of the expression levels of CD45 and CD68 were also conducted. The data were presented as mean ± SD (n = 3-6), ns means $P > 0.05$ (no significance), $^{*}P < 0.05$, $^{**}P < 0.01$, $^{***}P < 0.001$.

3.5 Gas@MPs Alleviates Hyperglycemia in T2DM Mice

Chronic hyperglycemia is often associated with abnormal lipid levels and a marked increase in inflammatory markers [47,48]. In this study, we assessed the four lipid components in pancreatic tissue, namely total cholesterol (TC), triglycerides (TG), high-density lipoprotein cholesterol (HDL-C), and low-density lipoprotein cholesterol (LDL-C) serum concentrations (Figures 5A-D). The results underscored the significant hypoglycemic and hypolipidemic effects of Gas@MPs. In contrast, the treatment groups with Gas and STZ exhibited no significant differences when compared to the blank control group. To evaluate the potential anti-inflammatory effects of Gas@MPs in diabetic mice, we employed enzyme-linked immunosorbent assay (ELISA) to measure the levels of tumor necrosis factor (TNF-α) and interleukin-1β (IL-β). The findings revealed that the administration of Gas@MPs resulted in a significant reduction of abnormal inflammation (Figure 5E,F), further emphasizing the therapeutic potential of Gas@MPs for diabetes. Although prior studies have indicated that Gas@MPs exert regulatory effects on CD45 and CD68 in the immunofluorescence layer, this study further corroborated these findings through immunohistochemical staining of pancreatic tissue. The results demonstrated that Gas@MPs effectively modulated the abnormal expressions of CD45 and CD68 (Figure 5I). Glycogen synthase kinase 3β (GSK-3β) is pivotal in glucose metabolism and glycogen synthesis. Specifically, GSK-3β, a serine/threonine kinase, acts as a negative regulator of insulin signaling, and its levels are typically elevated in diabetic patients [49,50]. The nuclear factor erythroid 2-related factor 2 (Nrf2) transcription factor not only regulates oxidative stress responses but also plays a crucial role in the inflammatory process. By regulating oxidative stress and inflammation mediated by the Nrf2/HO-1 signaling cascade, the occurrence of diabetic nephropathy can be effectively alleviated [51-53]. It is well-established that glucose transporter type 2 (Glut2) and insulin receptor substrate 1 (IRS1) are critical genes involved in dyslipidemia and insulin resistance. Glut2 facilitates glucose transport, while IRS1 plays a pivotal role in insulin signaling. Based on this understanding, we investigated whether Gas@MPs exert regulatory effects on

these significant factors in type 2 diabetes mellitus (T2DM). Our research findings indicate that Gas@MPs can effectively modulate the aberrantly elevated expression of GSK-3β protein induced by STZ, while also enhancing the expression levels of Nrf2, HO-1, Glut2, and IRS1 proteins (see Figure 5L). Consequently, we hypothesize that the improvement in blood lipid profiles and insulin resistance mediated by Gas@MPs may be achieved through the regulation of the GSK-3β/Nrf2/HO-1/Glut2/IRS1 signaling pathway. In order to conduct a more comprehensive verification of how Gas@MPs exert their antioxidant effects by modulating the GSK3β/Nrf2/HO-1 signaling axis, we also carried out protein gene knockout experiments to further enrich our research content. By knocking out the GSK-3β-/-, Nrf2-/-, and HO-1-/- protein genes, we found that under the same administration conditions, Gas@MPs were unable to effectively regulate the abnormal expression of corresponding proteins caused by STZ (as shown in Figure S1). This effectively verified that Gas@MPs achieve their antioxidant effects by regulating the GSK3β/Nrf2/HO-1 signaling axis.

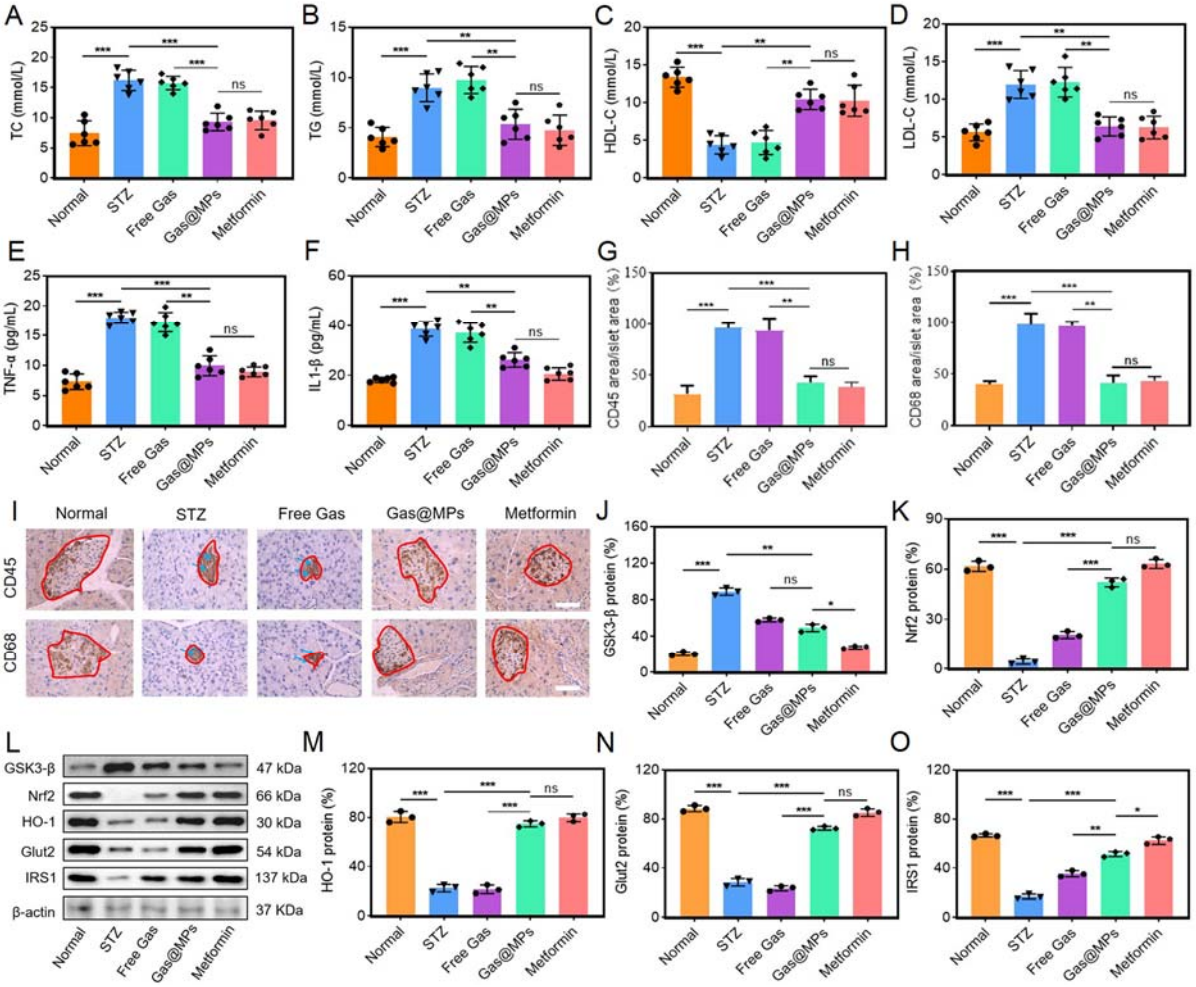
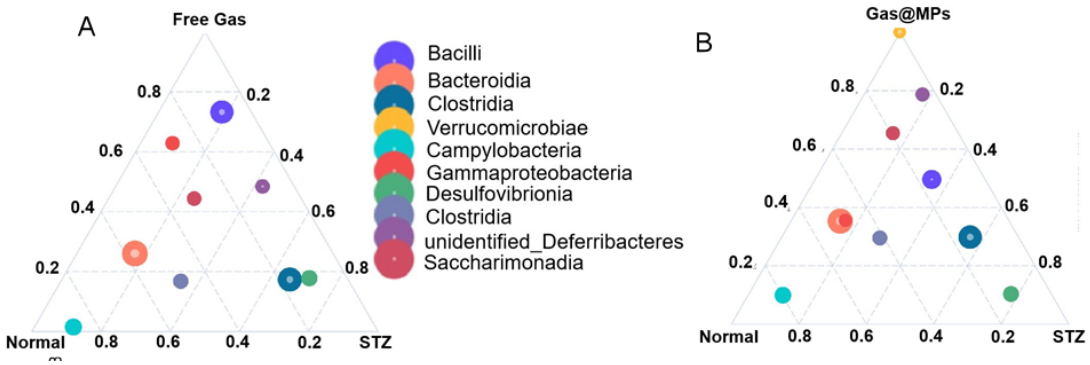


Fig.5 The regulatory effects of Gas@MPs on dyslipidemia and insulin resistance. (A-D) Evaluation of the four lipid parameters: triglycerides (TG), total cholesterol (TC), high-density lipoprotein cholesterol (HDL-C), and low-density lipoprotein cholesterol (LDL-C). (E, F) Evaluation of inflammatory markers TNF-α and IL-1β. (G, H) Quantitative analysis of the positive expressions of CD45 and CD68. (I) Immunohistochemical analysis of the expression of CD45 and CD68 proteins. (J,K) Quantitative analysis of the expression levels of GSK-3β and Nrf2 proteins. (L) Western blot evaluation of the GSK-3β/Nrf2/HO-1/Glut2/IRS1 signaling pathway. (M-O) Quantitative analysis of the expression levels of HO-1, Glut2 and IRS1 proteins. The data were presented as mean ± SD (n = 3-6), ns means $P > 0.05$ (no significance), $^{*}P < 0.05$, $^{**}P < 0.01$, $^{***}P < 0.001$.

3.6 Gas@MPs' Positive Regulation of Intestinal Microbiota Homeostasis

Scientific research evidence indicates a close interaction among obesity, diabetes, and intestinal microbial imbalance. Previous studies have demonstrated that Gas@MPs effectively regulate blood sugar levels. We hypothesize that they may play a role in remodeling the intestinal microbial environment induced by STZ. To verify this hypothesis, we conducted 16S rRNA sequencing on fecal samples from mice in different treatment groups. The ternary phase analysis of microbial distribution in the control group, STZ group, and Free Gas group revealed that the microbial distribution in both the STZ group and the Free Gas treatment group was relatively balanced, with no significant differences in the distribution of beneficial or harmful bacterial groups (Figure 6A). However, when comparing the control group, STZ group, and Gas@MPs group, beneficial bacterial groups such as Bacteroidia exhibited a distribution trend between the control group and the Gas@MPs group, with a relatively consistent distribution (Figure 6B). Bacteroides are a crucial component of the intestinal microbiota, capable of breaking down complex polysaccharides, such as dietary fibers, to assist in human digestion. They also produce short-chain fatty acids and participate in regulating intestinal immune responses, which is vital for maintaining homeostasis within the intestinal tract. In the analysis at the genus level (Figure 6C), the results indicated that the STZ intervention significantly increased the relative abundance of Helicobacter_ganmani and Bacteroides_sartorii, which are recognized as key harmful bacteria disrupting intestinal homeostasis. In contrast, the Gas@MPs treatment effectively ameliorated this disorder. Notably, the cluster heatmap analysis corroborated these findings at the phylum level, revealing that Gas@MPs significantly reduced the high expression of Bacteroides_sartorii (Figure 6F). The diversity analysis, conducted via principal coordinate analysis (PCoA), demonstrated that the Gas@MPs group exhibited the closest relationship with both the blank and metformin treatment groups (Figure 6D). Additionally, the non-metric multidimensional scaling (NMDS) results, which yielded a stress value of less than 0.2, emphasized the similarity of microbial communities between the Gas@MPs group and both the control and metformin treatment groups (Figure 6E). The strong correlation observed between these groups suggests that Gas@MPs significantly improves the bacterial community disorder induced by STZ.



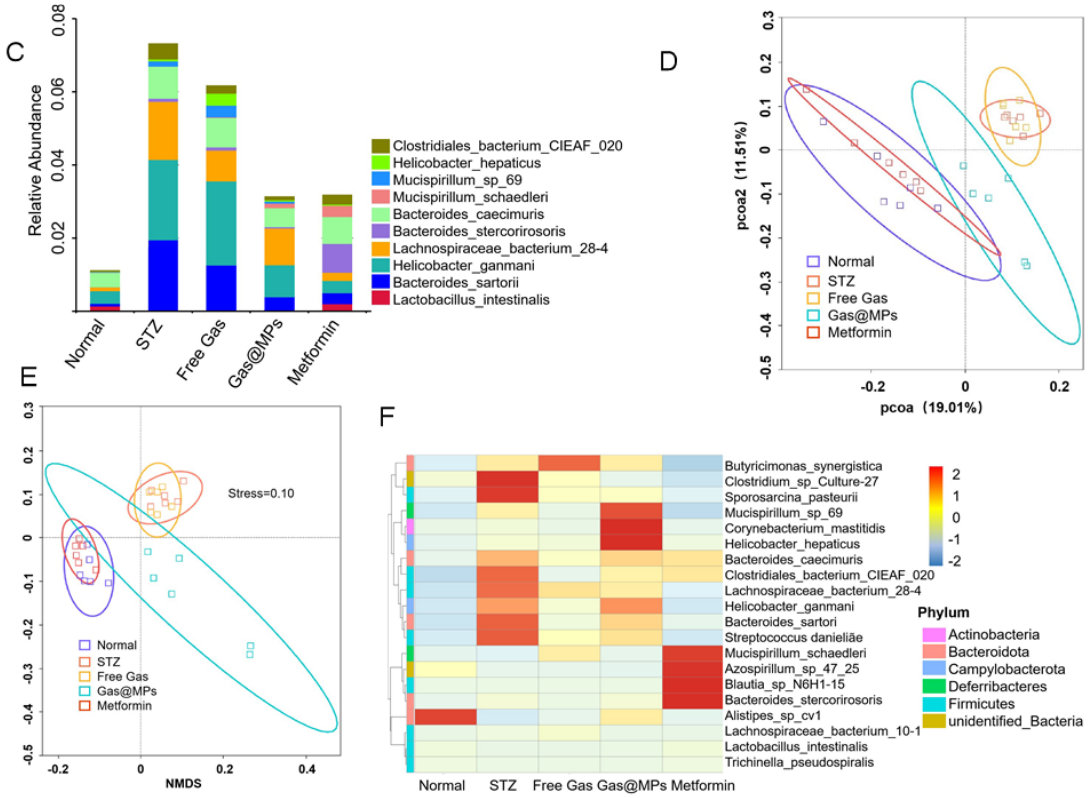


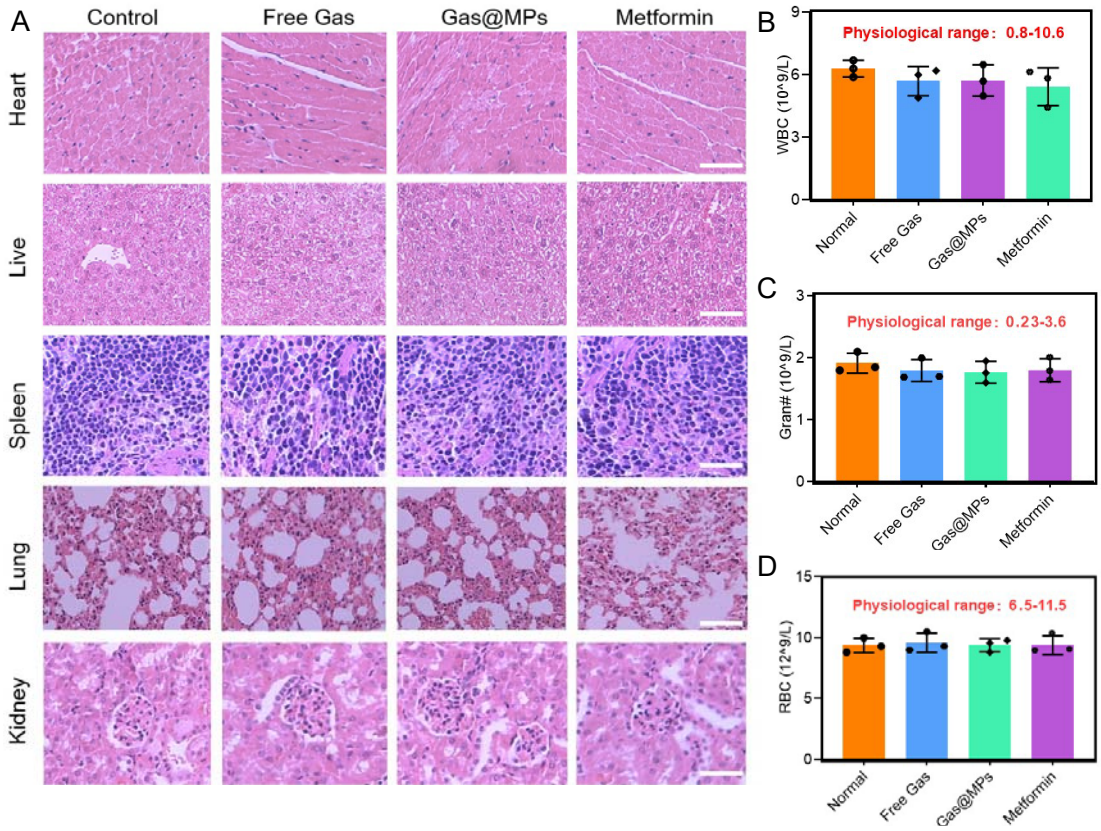
Fig.6 Gas@MPs significantly reshapes the homeostasis of gut microbiota. (A) A three-way analysis of core microbiota at the gate level was conducted among the Healthy Normal group, Free Gas group, and STZ treatment group. (B) Another three-way analysis of core microbiota at the gate level was performed in the Normal group, STZ group, and Gas@MPs treatment group. (C) The results include a histogram and heat map analysis of microbial communities. (D) Principal coordinate analysis was utilized to visualize the data. (E) Non-metric multidimensional scaling (NMDS) analysis was also conducted. (F) Finally, a cluster heatmap analysis was performed to illustrate the differences in the intestinal microbiota communities of mice.

We not only conducted a comparative analysis of the gut microbiota between the "Gas" group and the "Gas@MPs" group, and paid particular attention to the functional metabolism of the microorganisms. First of all, we have supplemented the comparative microbial structure: We re-analyzed the 16S rRNA sequencing data to compare the differential enrichment of key taxa between the Gas@MPs group and the free Gas group. We found that Gas@MPs more significantly enriched specific genera (e.g., Lactobacillus, Bifidobacterium, or Enterococcus) that are known to harbor high β-glucosidase activity, compared to free Gas (Figures S2). Secondly, we have added functional prediction/metagenomic analysis: To move beyond descriptive phenotyping, we performed metagenomic sequencing analysis to predict the functional potential of the microbial communities. Notably, we observed a significant upregulation of the “glycoside hydrolase” family (including β-glucosidase-encoding genes) in the Gas@MPs group compared to the free Gas group (Figures S3).

Based on these new data, we now propose that compared to free Gas, Gas@MPs may act as a “prebiotic-like” modulator that selectively enriches β-glucosidase-producing microbiota, thereby enhancing the biotransformation of Gas. This comparative approach has successfully elevated our microbiota analysis from a descriptive observation to a mechanistic hypothesis-generation stage.

3.7 The Excellent Biocompatibility and Biostability of Gas@MPs

Our previous research has demonstrated through in vitro cell experiments that Gas@MPs are non-toxic and exhibit no adverse effects on cells. The excellent safety profile of the substance is well established as a fundamental basis for its application. However, given that the Gas@MPs microspheres we investigated were administered orally to animals, it is essential to monitor the metabolic conditions of relevant organs and physiological indicators following oral administration. In this study, we further confirmed the biological safety of the treatments by assessing serum functional indicators and performing H&E staining in mice. Initially, free Gas, Gas@MPs, and metformin were administered orally to the mice, followed by an examination of potential abnormalities in major organ tissues and related physiological function indicators. The H&E staining results indicated that, compared to the control group, no abnormalities were detected in the major organs (heart, liver, spleen, lung, and kidney) across the various treatment groups (Figure 7A). Additionally, key serum physiological indices were evaluated, including white blood cell count (WBC), absolute neutrophil count (Gran#), red blood cell count (RBC), lymphocyte count (Lymph#), hematocrit (HCT), and hemoglobin (HGB). All relevant indicators remained within the standard physiological range (Figure 7B-G). These findings indicate that both free Gas and Gas@MPs exhibit good biocompatibility and biological safety. The excellent safety characteristics of Gas@MPs, coupled with its efficacy in managing abnormal blood sugar levels resulting from insulin resistance, suggest a promising potential for further development in diabetes treatment.



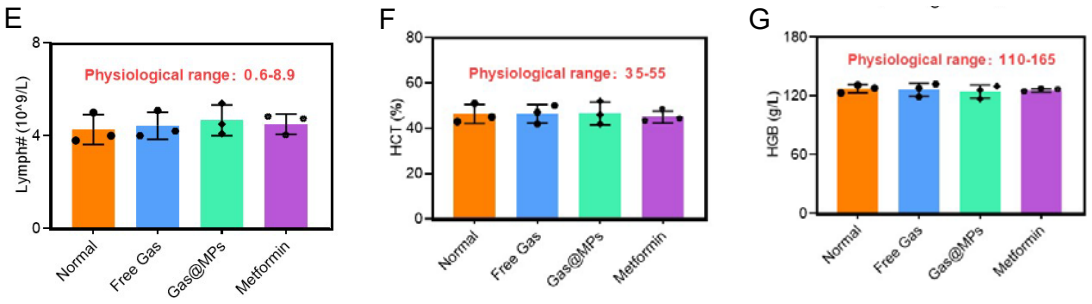


Fig.7 Safety assessment of Gas@MPs in mice. (A) H&E staining analysis of major organs treated with different samples. (B-G) white blood cell (WBC); neutrophil count (Gran#), red blood cell count (RBC), lymphocyte count (Lymph#), hematocrit (HCT), and hemoglobin (HGB), the values were represented as mean ± SD (n = 3).

3.8 Optimization of Preparation Technology of Microspheres

The microspheres prepared using SA and LMP at varying concentrations were examined under a microscope (Figure 8A). The observations revealed that at a concentration of 1.5% SA and 0.5% LMP, the microspheres exhibited a complete and uniform spherical morphology, particularly the Gas@MPs microsphere. Following the determination of the optimal concentrations, the ideal injection distance was found to be 16 cm, with a voltage of 16 kV and an optimal $CaCl_2$ concentration of 2% to achieve the desired microspheres (Figure 8B).

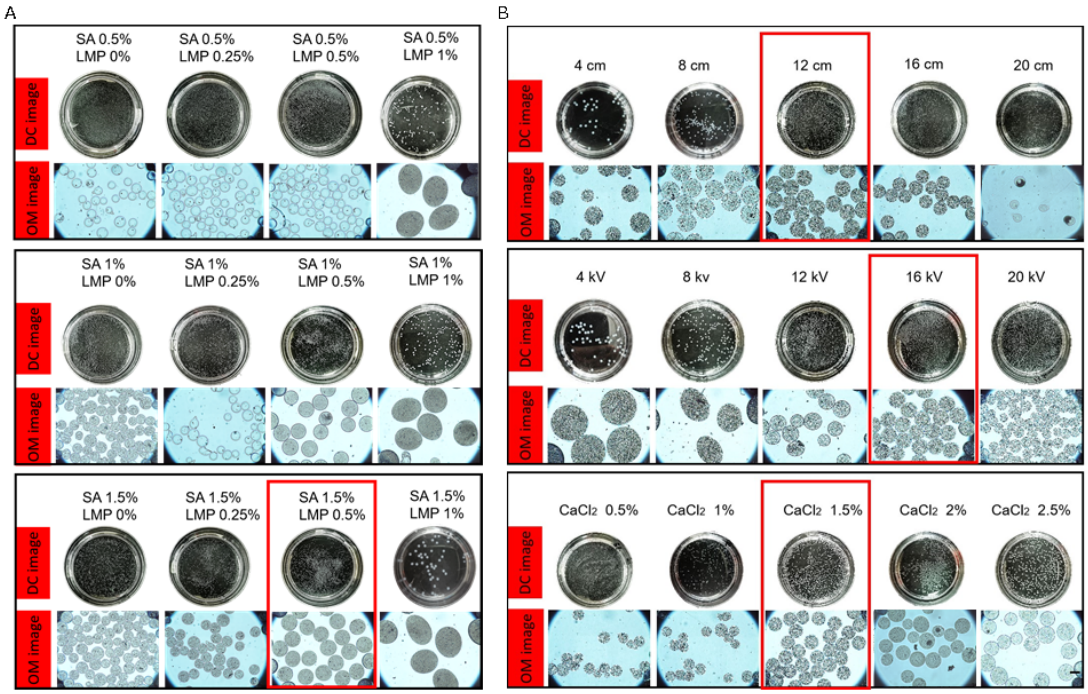


Fig.8 Preparation and process optimization of Gas@MPs Microspheres. (A) Effect of sodium alginate and pectin concentration ratio on microsphere shape. Scale bars :150 μm. (B) From top to bottom were injection distance, voltage and $CaCl_2$ concentration respectively. Scale bars :150 μm.

4. Conclusion

In our study, we first verified the physiological activity of Gas. Further, the prepared Gas@MPs not only exhibited excellent stability and pH responsiveness, but also could minimize the decomposition of gas in gastric acid, ensuring targeted release in the intestine and having a positive therapeutic effect on diabetes. This novel targeted drug delivery strategy is expected to provide more effective and more tolerable treatment

options for diabetic patients and bring broad prospects for the application of Gas.

Notes

The authors declare no competing financial interest.

Acknowledgements

This work was supported by The PhD start-up fund of Guizhou University of Traditional Chinese Medicine ([2025] No. 16). Zhejiang Provincial Natural Science Foundation for Young Scientists (LQN25H280004).

Data availability statement

Data available on request from the authors.

References

[1]. J. E. Morley, The diabetic brain. Nat. Rev. Endocrinol. 13(2017)570-571.

[2]. H. J. Anders, T. B. Huber, B. Isermann, et al., CKD in diabetes: diabetic kidney disease versus nondiabetic kidney disease. Nat. Rev. Nephrol. 14(2018)361-377.

[3]. T. T. Wang, L. Zheng, S. G. Wang, et al., Anti-diabetic and anti-hyperlipidemic effects of sea cucumber (Cucumaria frondosa) gonad hydrolysates in type II diabetic rats. Food Sci. Hum. Wellness. 11(2022)1614-1622.

[4]. A. T. Hattersley, K. A. Patel, Htd2 deficiency-associated suppression of α-lipoic acid production provokes mitochondrial dysfunction and insulin resistance in adipocytes. Diabetologia. 60(2017)769-777.

[5]. M. Byndloss, S. Devkota, F. Duca, et al., The Gut Microbiota and Diabetes: Research, Translation, and Clinical Applications-2023 Diabetes, Diabetes Care, and Diabetologia Expert Forum. Diabetes Care. 73(2024)1391-1410.

[6]. J. J. Chamberlain, K. Doyle-Delgado, L. Peterson, et al., Diabetes technology: review of the 2019 american diabetes association standards of medical care in diabetes. Ann Intern Med. 171(2019)415-420.

[7]. A. L. Birkenfeld, V. Mohan, Prediabetes remission for type 2 diabetes mellitus prevention. Nat. Rev. Endocrinol. 20(2024)441-442.

[8]. K. J. Lipska, I. B. Hirsch, M. C, Riddle, et al., Human Insulin for Type 2 Diabetes: An effective, less-expensive option. JAMA. 318(2017)23-24.

[9]. L. J. Scott, Insulin Glargine/Lixisenatide: A Review in Type 2 Diabetes. Drugs. 77(2017)1353–1362.

[10]. W. T. Cefalu, G. Arreaza-Rubin, Engineering an insulin complex to treat diabetes. NEJM. 390(2024)2214-221.

[11]. X. R. He, X. F. Chen, Y. Yang, et al., The role of gastrodin in the management of CNS-related diseases: Underlying mechanisms to therapeutic perspectives. Phytother. Res. 38(2024)5107-5133.

[12]. P. Krol, L. Byczynski, M. Sochacka-Piętal, Hydrophilic polyurethane films containing gastrodin as potential temporary biomaterials. Prog. Org. Coat. 178(2023)107481.

[13]. W. X. Qin, J. Q. Du, F. Wang, et al., Gastrodin: a potential natural product for the prevention and treatment of cerebral ischemia-reperfusion injury. Front Pharmacol. 16(2025)1554170.

[14]. H. L. Zhang, Z. H. Zhao, P. Liu, et al., Gastrodin enhances stress resilience through promoting Wnt/β-Catenin-dependent neurogenesis. J Adv Res. 25(2025)S2090-1232.

[15]. Y. F. Li, B. W. Zhu, T. Chen, et al., Glutathione-responsive nanoplatforms trigger gaseous intervention of intestinal inffammation through TLR4/MD2/MyD88/NF-κB/iNOS pathway activation and gut microbiota modulation. Chem. Eng. J. 493(2024)152849.

[16]. L. Aguero, D. Zaldivar-Silva, L. Pena, et al., Alginate microparticles as oral colon drug delivery device: A review. Carbohydr. Polym. 168(2017)32-43.

[17]. D. Aycan, I. Gul, V. Yorulmaz, N. Gelatin microsphere-alginate hydrogel combined system for sustained and gastric targeted delivery of 5-fluorouracil. Int. J. Biol. Macromol. 255(2024)128022.

[18]. K. L. Chen, H. Zhang, Alginate/pectin aerogel microspheres for controlled release of proanthocyanidins. Int. J. Biol. Macromol. 136(2019)936-943.

[19]. F. Fathordoobady, M. Jarzębski, A. Pratap-Singh, et al., Encapsulation of betacyanins from the peel of red dragon fruit (Hylocereus polyrhizus L.) in alginate microbeads. Food Hydrocoll. 113(2021)106535.

[20]. J. Chudzinska-Skorupinska, A. Wawrzynczak, A. Feliczak-Guzik, Carbohydrate-based polymer nanocarriers for environmentally friendly applications. Adv. Colloid Interface Sci. 338(2025)103415.

[21]. N. Angel, S. N. Li, L. Y. Kong, Emerging applications of nanofibers electrospun from carbohydrate polymers. Journal of Future Foods. 4(2024)289-299.

[22]. X. M. Guo, H. L. Chen, Z. M. Wang, et al., Sugarcane molasses-induced gelation of low-methoxy pectin. Ind. Crop. Prod. 205(2023)117509.

[23]. Q. H. Ouyang, Y. Zhao, K. Y. Xu, et al., Hyaluronic acid receptor-mediated nanomedicines and targeted therapy. Small Methods. 8(2024)2400513.

[24]. W. H. Lee, W. Kim, Self-assembled hyaluronic acid nanoparticles for the topical treatment of inflammatory skin diseases: Beyond drug carriers. JCR. 366(2024)114-127.

[25]. Z. J. Luo, Y. Dai, H. L. Gao, Development and application of hyaluronic acid in tumor targeting drug delivery. Acta Pharm Sin B. 9(2019)1099-1112.

[26]. X. Y. Dong, Y. Y. Suo, J. Yu, et al., Biomimetic nanoparticles simultaneously targeting modulation of lipid metabolism and phenotype of macrophages for programmed atherosclerosis management. ACS Nano. 19(2025)25628-25644.

[27]. T. Liu, X. M. Chen, J. Y. Sun, et al., Palmitic acid-induced podocyte apoptosis via the reactive oxygen species dependent mitochondrial pathway. Kidney Blood Press Res. 43(2018) 206-219.

[28]. F. X. Luo, B. W. Zhu, D. Wu, et al., Construction of phlorotannin-based nanoparticles for alleviating acute liver injury. ACS Appl. Mater. Inter. 15(2023)47338-47349.

[29]. X. B. Kong, M. Gao, Y. T. Liu, et al., GSDMD-miR-223-NLRP3 axis involved in B(a)P-induced inflammatory injury of alveolar epithelial cells. Ecotox Environ Safe. 232(2022)113286.

[30]. Y. Xu, B. W. Zhu. R. Sun, et al., Colon-targeting angelica sinensis polysaccharide nanoparticles with dual responsiveness for alleviation of ulcerative colitis. ACS Appl. Mater. Interfaces. 15(2023)26298-26315.

[31]. B. Dou, W. J. Hu. M. K. Song, et al., Anti-inflammation of Erianin in dextran sulphate sodium-induced ulcerative colitis mice model via collaborative regulation of TLR4 and STAT3. Chem. Biol. Interact. 324(2020)109089.

[32]. Y. Xu, X. C. Wang, W. Jiang, et al., Angelica sinensis polysaccharides modified selenium nanoparticles for effective prevention of acute liver injury. Int. J. Biol. Macromol. 1(2024)130321.

[33]. V. S. Tanwar, M. A. Reddy, S. Das, et al., Natarajan, 451-p: palmitic acid–induced lncrna parail regulates inflammation via restricting hur localization to cytoplasm in human monocytes and macrophages. Diabetes. 71(2022)0012-1797.

[34]. T. T. Qiu, X. Yang, J. Z. Wang, et al., Obesity-induced elevated palmitic acid promotes inflammation and glucose metabolism disorders through Gprs/NF-KB/KLF7 pathway. Nutr. Diabetes. 12(2022)2044-4052.

[35]. H. Wood, Mitochondrial dysfunction manifests in the early stages of alzheimer disease. Nat. Rev. Neurol. 16(2020)2045-2322.

[36]. Q. Zhu, R. P. Zhu, J. F. Jin, Neutral ceramidase-enriched exosomes prevent palmitic acid-induced insulin resistance in H4IIEC3 hepatocytes. FEBS open bio. 6(2016)2211-5463.

[37]. H. J. Anders, T. B. Huber, B. Isermann, et al., CKD in diabetes: diabetic kidney disease versus nondiabetic kidney disease. Nat. Rev. Nephrol. 14(2018)361-377.

[38]. S. Z. Varghese, P. Winocour, Managing diabetic kidney disease. Brit. Med. Bull. 125(2018)55-66.

[39]. X. Y. Dong, D. H. Lin, J. Z. Sheng, et al., Intrauterine hyperglycemia induces liver inflammation in mouse male offspring. Int. Immunopharmacol. 99(2021)107974.

[40]. E. G. Butkowski, H. F. Jelinek, Hyperglycaemia, oxidative stress and inflammatory markers. Redox Report. 22(2017)257-264.

[41]. S. H. Hædersdal, A. Lund, F. K. Knop, et al., The role of glucagon in the pathophysiology and treatment of type 2 diabetes. Mayo Clinic Proceedings. 93(2018)217-239.

[42]. S. S. Hua, W. Y. Li, D. W. Zheng, et al., The proliferating cell nuclear antigen gene (PCNA) plays a key role in ovarian development in the ridgetail white prawn, Exopalaemon carinicauda. Aquacult. Rep. 36(2024)102170.

[43]. M. R. Al-Shathly, S. S. Ali, N. N. Ayuob, Zingiber officinale preserves testicular structure and the expression of androgen receptors and proliferating cell nuclear antigen in diabetic rats. Andrologia. 5(2020)13528.

[44]. Y. H. Lee, M. Y. Wang, X. X. Yu, et al., Glucagon is the key factor in the development of diabetes. Diabetologia. 59(2016)1372–1375.

[45]. S. Barac, R. R. Onofrei, C. Lazureanu, R. Barna, A. Tutelca, A. L. Rata, An in vivo observational histological study of peripheral arterial damage in patients with acute limb ischemia in sars-cov-2 infection. Diagnostics. 12(2022)488.

[46]. H. Y. Zeng, W, R. Green, M. O. M. Tso, Microglial activation in human diabetic retinopathy. Arch Ophthalmol. 126(2008)227-232.

[47]. N. A. Santos, R. L. Ferretti, Inflammatory status assessment in critically ill patients with hyperglycemia. Clin Nutr. 37(2018)S172.

[48]. T. M. J. S. Kumari, G. Revathy, D. Prabha, A Review of inflammatory markers in metabolic syndrome. Int. J. Life. Sci. Pharm. 13(2023)159-165.

[49]. Y. X. Sun, H. Shi, S. Q. Yin, et al., Human mesenchymal stem cell derived exosomes alleviate type 2 diabetes mellitus by reversing peripheral insulin resistance and relieving β-cell destruction. ACS nano. 12(2018)7613-7628.

[50]. H. J. Anders, T. B. Huber, B. Isermann, et al., CKD in diabetes: diabetic kidney disease versus nondiabetic kidney disease. Nat. Rev. Nephrol. 14(2018)361-377.

[51]. F. G. Xiao, S. L. Rui, X. H. Zhang, et al., Accelerating diabetic wound healing with Ramulus Mori (Sangzhi) alkaloids via NRF2/HO-1/eNOS pathway. Phytomedicine. 134(2024)155990.

[52]. H. Wang, X. Y. Yu, D. W. Liu, et al., VDR activation attenuates renal tubular epithelial cell ferroptosis by regulating Nrf2/HO-1 signaling pathway in diabetic Nephropathy. Adv. Sci. 11(2024)2305563.

[53]. S. Y. Zhang, B. H. Peng, Y. Qi, et al., Dual response Hst1@CBTC hydrogel promoting diabetic wounds healing by improving mitochondrial autophagy and inhibiting ferroptosis via Nrf2/HO-1. Chem. Eng. J. 492(2024)152358.